Science Advances
AAAS

Supplementary Materials for

Imprint of chondrule formation on the K and Rb isotopic compositions of carbonaceous meteorites

Nicole X. Nie*, Xin-Yang Chen, Timo Hopp, Justin Y. Hu, Zhe J. Zhang, Fang-Zhen Teng, Anat Shahar, Nicolas Dauphas

*Corresponding author. Email: nnie@carnegiescience.edu

Published 1 December 2021, *Sci. Adv.* **7**, eabl3929 (2021)
DOI: 10.1126/sciadv.abl3929

This PDF file includes:

Supplementary Text

Calculation of the chondrule cooling rate

We present here the details of our model relating chondrule cooling rate to element condensation and isotopic fractionation (see (*7*, *58*, *81*) for similar modeling efforts). The initial temperature is the average peak temperature of porphyritic chondrules (1550 °C or 1823 K). We assume that at the beginning, chondrules and the surrounding gas are in elemental and isotopic equilibrium, and a linear cooling rate is then applied to the system. We assume that the chondrule melt and vapor form a closed system. As the system cools, alkali elements in the vapor become supersaturated and condense into the melt, reducing the vapor pressure. With fast cooling, the rate of condensation is insufficient to track the rapidly decreasing equilibrium vapor pressure and large oversaturation develops. With slow cooling, the rate of condensation allows the partial vapor pressure to track the equilibrium vapor pressure and no supersaturation can develop.

Potassium is used as an example here, but the formalism can be applied to other elements. The equilibrium vapor pressure of gaseous K (the dominant vapor species for K) can be calculated using the following reaction,

$$\mathrm{KO}_{0.5(s)} \rightleftarrows \mathrm{K}_{(g)} + \frac{1}{4}\mathrm{O}_{2(g)}, \text{ (S1)}$$

The equilibrium constant (K_{K}) can be written as,

$$K_{\mathrm{K}} = \frac{P_{\mathrm{K,eq}} {P_{\mathrm{O}_2}}^{1/4}}{a_{\mathrm{KO}_{0.5}}}, \text{ (S2)}$$

where $P_{\mathrm{K,eq}}$ and P_{O_2} are the equilibrium vapor pressures of K and O_2, respectively, and $a_{\mathrm{KO}_{0.5}}$ is the activity of $\mathrm{KO}_{0.5}$ in melt. The activity $a_{\mathrm{KO}_{0.5}}$ can be rewritten as the product of activity coefficient ($\chi_{\mathrm{KO}_{0.5}}$) and the concentration, which is the mole fraction of the species among all oxide species of the molten chondrule ($n_{\mathrm{KO}_{0.5}}/n_{\mathrm{Ox,tot}}$; with SiO_2, TiO_2, Al_2O_3, FeO, Cr_2O_3, MnO, MgO, NiO, CoO, CaO, $NaO_{0.5}$, $KO_{0.5}$, and $RbO_{0.5}$ the oxides considered and n the mol density in mol m^{-3}). Equilibrium constants use pressure in bar, but here we convert it to SI unit Pa,

$$K_{\mathrm{K}} = \frac{\frac{P_{\mathrm{K,eq}}}{10^5}\left(\frac{P_{\mathrm{O}_2}}{10^5}\right)^{1/4}}{\chi_{\mathrm{KO}_{0.5}}\ (n_{\mathrm{KO}_{0.5}}/n_{\mathrm{Ox,tot}})}. \text{ (S3)}$$

Rearranging the equation to solve for the equilibrium vapor pressure of K,

$$P_{\mathrm{K,eq}} = \frac{10^{25/4}}{n_{\mathrm{Ox,tot}}} \frac{K_{\mathrm{K}}\ \chi_{\mathrm{KO}_{0.5}}}{{P_{\mathrm{O}_2}}^{1/4}} n_{\mathrm{KO}_{0.5}}. \text{ (S4)}$$

The condensation flux can be calculated using the Hertz-Knudsen equation (*7*, *58*), which takes the form,

$$J_i = \frac{\gamma_i\left(P_{i,eq} - P_i\right)}{\sqrt{2\pi m_i RT}}, \text{ (S5)}$$

where J_i is the net condensation flux in the unit of mol m^{-2} s^{-1}, i can be an element or an isotope, γ_i is the condensation coefficient, $P_{i,eq}$ and P_i are equilibrium vapor pressure and actual partial vapor pressure of i in the gas in unit of Pa, respectively, m_i is the molar mass of the gas species in kg mol^{-1}, R is the gas constant that has a value of 8.314 m^3 Pa K^{-1} mol^{-1}, and T is temperature in K. We assume that the gas surrounding the chondrule is well mixed and follows the ideal gas law, so that the total moles of K in the gas at any given time is

$$n_{\mathrm{K}} = \frac{P_{\mathrm{K}} V}{RT} = P_{\mathrm{K}} \frac{4\pi \mathcal{R}^3}{3RT}, \text{ (S6)}$$

where V is the volume and $\mathcal{R}$ the radius of the gas parcel. Combining Eq. S6 and Eq. S5, and taking derivatives on both sides, one can write,

$$\frac{V}{RT} dP_{\mathrm{K}} - \frac{P_{\mathrm{K}} V}{RT^2} dT = \frac{\gamma_{\mathrm{K}} \left(P_{\mathrm{K,eq}} - P_{\mathrm{K}}\right)}{\sqrt{2\pi m_{\mathrm{K}} RT}} 4\pi r^2 dt, \text{ (S7)}$$

where r is the radius of molten chondrule in meter, which is approximately constant during condensation as only the most volatile elements are in the vapor phase. By rearranging the above equation, one gets,

$$\frac{1}{T} \frac{dP_{\mathrm{K}}}{dt} - \frac{P_{\mathrm{K}}}{T^2} \frac{dT}{dt} = 3\gamma_{\mathrm{K}} \left(P_{\mathrm{K,eq}} - P_{\mathrm{K}}\right) \frac{r^2}{\mathcal{R}^3} \sqrt{\frac{R}{2\pi m_{\mathrm{K}} T}}. \text{ (S8)}$$

In a closed system, the total amount of K is always equal to the sum of K in the molten chondrule and in the gas,

$$P_{\mathrm{K}} \frac{4\pi \mathcal{R}^3}{3RT} + n_{\mathrm{KO_{0.5}}} \frac{4\pi r^3}{3} = n_{\mathrm{K,tot}} \frac{4\pi r^3}{3}, \text{ (S9)}$$

where n is in mol m^{-3}. Equation S9 can be simplified as,

$$P_{\mathrm{K}} = RT \left(n_{\mathrm{K,tot}} - n_{\mathrm{KO_{0.5}}}\right) \frac{r^3}{\mathcal{R}^3}. \text{ (S10)}$$

Taking the derivatives on both sides, it follows,

$$dP_{\mathrm{K}} = R \left(n_{\mathrm{K,tot}} - n_{\mathrm{KO_{0.5}}}\right) \frac{r^3}{\mathcal{R}^3} dT - RT \frac{r^3}{\mathcal{R}^3} dn_{\mathrm{KO_{0.5}}}. \text{ (S11)}$$

Inserting Eqs. S4, S10, and S11 into Eq. S8, we get,

$$\frac{dn_{\mathrm{KO_{0.5}}}}{dt} = \frac{3\gamma_{\mathrm{K}}}{r} \sqrt{\frac{RT}{2\pi m_{\mathrm{K}}}} \left[\frac{r^3}{\mathcal{R}^3} n_{\mathrm{K,tot}} - \left(\frac{r^3}{\mathcal{R}^3} + \frac{10^{25/4}}{n_{\mathrm{Ox,tot}}} \frac{K_{\mathrm{K}} \chi_{\mathrm{KO_{0.5}}}}{RT \, {P_{\mathrm{O_2}}}^{1/4}}\right) n_{\mathrm{KO_{0.5}}}\right]. \text{ (S12)}$$

Imposing a linear cooling rate on the condensation by assuming

$$T(t) = T_0 + \Phi t, \text{ (S13)}$$

and replacing $n_{\mathrm{KO}_{0.5}}$ with n_{K}, we have,

$$\frac{dn_{\mathrm{K}}}{dT} = \frac{3\gamma_{\mathrm{K}}}{r\Phi}\sqrt{\frac{RT}{2\pi m_{\mathrm{K}}}}\left[\frac{r^3}{\mathcal{R}^3}n_{\mathrm{K,tot}} - \left(\frac{r^3}{\mathcal{R}^3} + \frac{10^{25/4}}{n_{\mathrm{Ox,tot}}}\frac{K_{\mathrm{K}}\chi_{\mathrm{K}}}{RT\,P_{\mathrm{O}_2}{}^{1/4}}\right)n_{\mathrm{K}}\right]. \text{(S14)}$$

By dividing both sides by the total amount of K, the differential equation describing how the condensed fraction evolves as a function of temperature takes the form,

$$\frac{df_{\mathrm{K}}}{dT} = \frac{3\gamma_{\mathrm{K}}}{r\Phi}\sqrt{\frac{RT}{2\pi m_{\mathrm{K}}}}\left[\frac{r^3}{\mathcal{R}^3} - \left(\frac{r^3}{\mathcal{R}^3} + \frac{10^{25/4}}{n_{\mathrm{Ox,tot}}}\frac{K_{\mathrm{K}}\chi_{\mathrm{K}}}{RT\,P_{\mathrm{O}_2}{}^{1/4}}\right)f_{\mathrm{K}}\right]. \text{(S15)}$$

The partial differential equations S14 and S15 apply to both elements and isotopes. In the equations, n_{K} and f_{K} are the amount and the fraction of K in the molten chondrule (*i.e.*, the condensed fraction of K), respectively, T is temperature in K, Φ is cooling rate in K s^{-1}, R is the gas constant 8.314 m^3 Pa K^{-1} mol^{-1}, and m_{K} is the molar mass of K (39.098 g mol^{-1}). We assume the radius of chondrule (r) to be a constant value of 0.5 mm, which is typical for chondrules (*82*) and was used in previous models of chondrule formation (*e.g.*, (*55*, *70*, *81*)). The radius of the gas ($\mathcal{R}$) surrounding the molten chondrule is set by the fraction of K in the chondrule melt ($f_{\mathrm{K},0}$) at peak temperature (T_0) assuming gas-melt equilibrium,

$$\mathcal{R} = r\,\left[\frac{(1-f_{\mathrm{K},0})}{f_{\mathrm{K},0}}\frac{n_{\mathrm{Ox,tot}}}{10^{25/4}}\frac{RT_0\,P_{\mathrm{O}_2}{}^{1/4}}{K_{\mathrm{K}}\chi_{\mathrm{K}}}\right]^{1/3}. \text{(S16)}$$

The peak temperature T_0 is set at 1550 °C or 1823 K; the average peak temperature of porphyritic chondrules (*63*, *64*). Chondrules have different textures for which different peak melting temperatures are invoked (e.g., (*63*, *64*, *67*)), but the majority of chondrules (~80%) are porphyritic (*83*). We calculate that $\mathcal{R}$ must be between 0.04 and 0.2 m (Fig. S3), in agreement with previous estimates (*e.g.*, (*48*, *54*, *84*)) . $n_{\mathrm{Ox,tot}}$ in mol m^{-3} is assumed to be constant during condensation and is calculated by assuming a bulk CI-composition. The assumption that this value is constant is realistic because alkali elements only represent a small fraction of CI components ($NaO_{0.5}$, $KO_{0.5}$ and $RbO_{0.5}$ represent only 2 mol% of all oxides in total). The product $K_{\mathrm{K}}\chi_{\mathrm{K}}\gamma_{\mathrm{K}}$ depends on temperature, and the value can be determined experimentally. In this work we use the data from (*62*), which gives the latest constraints on alkali element evaporation/condensation kinetics based on vacuum evaporation experiments. In the above equations, the evaporation coefficient γ_{K} has to be separated from $K_{\mathrm{K}}\chi_{\mathrm{K}}$. We assume a constant value of 0.1 for γ_{K} (and for γ_{Na} and γ_{Rb}) and we use the following relationships (*62*),

$$\ln(\chi_{\mathrm{K}}\,\gamma_{\mathrm{K}}) = -29265/\mathrm{T} + 3.4593, \text{(S17)}$$
$$\ln(\chi_{\mathrm{Na}}\,\gamma_{\mathrm{Na}}) = -22239/\mathrm{T} + 2.4947, \text{(S18)}$$
$$\ln(\chi_{\mathrm{Rb}}\,\gamma_{\mathrm{Rb}}) = -35020/\mathrm{T} + 7.4795. \text{(S19)}$$

The oxygen partial pressure P_{O_2} in Pa was calculated by assuming a constant oxygen fugacity of IW−1.5 (*54*, *55*), which varies with temperature following the relationship (*85*),

$$Log_{10}P_{\mathrm{O}_2} = 3.5 - \frac{27489}{T} + 6.072. \text{(S20)}$$

Using Eq. S15, one can calculate the fraction of an element condensed as a function of temperature for various cooling rates. Applying Eq. S14 to isotopes, one can calculate the condensed amount of each isotope and the isotopic composition of the condensate. We used Mathematica to solve these partial differential equations numerically.

Test of the numerical model: instantaneous cooling

We solved the partial differential equations describing condensation in the time (Eq. S12) and temperature domains (Eq. S14) and the results are consistent. The differential equations were solved numerically using Mathematica as they do not have simple analytical solutions. In this section, we consider the special case of instantaneous cooling, whereby a system that is at equilibrium at temperature T_0, evolves to a new equilibrium when the temperature suddenly drops to a lower temperature T_e. Such a cooling scheme simplifies the equations and allows us to derive an analytical solution, which can be compared to the numerical solution, thereby providing a means of testing the numerical model.

We consider a closed system comprising a well-mixed melt sphere surrounded by a concentric shell of well-mixed vapor (similar to the chondrule setting). As a result of the sudden drop in temperature, the vapor that was at equilibrium with the liquid at T_0 becomes supersaturated, resulting in condensation that will continue until liquid and vapor reach equilibrium at T_e. Bourdon and Fitoussi (*86*) developed an analytical equation for a similar scenario. They used Eq. B23 from Dauphas *et al.* (*8*) to calculate the instantaneous isotopic fractionation factor associated with condensation from a supersaturated vapor medium. That formula, however, assumes that the isotopic composition of each increment of condensate is solely set by the condensation flux, which is not the case here, unless transport in the liquid is diffusion limited. We assume instead that the equilibrium vapor pressure is set by the bulk liquid, meaning that the condensing atoms can mix instantaneously with atoms already in the liquid. Furthermore, Bourdon and Fitoussi (*86*) did not track the temporal evolution of the system. Below, we solve Eq. S12 for instantaneous cooling. We allow for instantaneous mixing in the liquid and track the temporal evolution of the system.

To simplify the expressions, we start by replacing $n_{\mathrm{KO0.5}}$ with the notation n_{K} (the amount of K in the condensate in mol m^{-3}) in Eq. S12,

$$\frac{dn_{\mathrm{K}}}{dt} = \frac{3\gamma_{\mathrm{K}}}{r}\sqrt{\frac{RT}{2\pi m_{\mathrm{K}}}}\left[\frac{r^3}{\mathcal{R}^3}n_{\mathrm{K,tot}} - \left(\frac{r^3}{\mathcal{R}^3} + \frac{10^{25/4}}{n_{\mathrm{Ox,tot}}}\frac{K_{\mathrm{K}}\,\chi_{\mathrm{K}}}{RT\,{P_{\mathrm{O_2}}}^{1/4}}\right)n_{\mathrm{K}}\right]. \quad \text{(S21)}$$

The temperature T is changed instantaneously and the system stays at that temperature afterwards, so the only time-dependent variable is n_{K}. We can simplify this equation by using the notation $n_{\mathrm{K},e}$, which is the amount of K that would be in the condensate (in mol m^{-3}) if the system was allowed to evolve for long enough to reach equilibrium at T_e (*i.e.*, $dn_{\mathrm{K},e}/dt = 0$),

$$n_{\mathrm{K},e} = \frac{r^3 n_{\mathrm{K,tot}}}{\mathcal{R}^3}\Big/\left(\frac{r^3}{\mathcal{R}^3} + \frac{10^{25/4}}{n_{\mathrm{Ox,tot}}}\frac{K_{\mathrm{K}}\,\chi_{\mathrm{K}}}{RT\,{P_{\mathrm{O_2}}}^{1/4}}\right). \quad \text{(S22)}$$

Equation S21 can then be rewritten as,

$$\frac{dn_{\mathrm{K}}}{dt} = 3\gamma_{\mathrm{K}}\sqrt{\frac{RT}{2\pi m_{\mathrm{K}}}}\frac{r^2}{\mathcal{R}^3}n_{\mathrm{K,tot}}\left(1-\frac{n_{\mathrm{K}}}{n_{\mathrm{K},e}}\right). \text{(S23)}$$

Rearranging and integrating the equation from time zero ($t = 0$, $n_{\mathrm{K}} = n_{\mathrm{K},0}$) to time t, we have,

$$\frac{n_{\mathrm{K}}}{n_{\mathrm{K},e}} = 1-\left(1-\frac{n_{\mathrm{K},0}}{n_{\mathrm{K},e}}\right)e^{-3\gamma_{\mathrm{K}}\sqrt{\frac{RT}{2\pi m_{\mathrm{K}}}}\frac{r^2}{\mathcal{R}^3}\frac{n_{\mathrm{K,tot}}}{n_{\mathrm{K},e}}t}. \text{(S24)}$$

Introducing the notations $f_0 = n_{\mathrm{K},0}/n_{\mathrm{K,tot}}$, $f = n_{\mathrm{K}}/n_{\mathrm{K,tot}}$, and $f_e = n_{\mathrm{K},e}/n_{\mathrm{K,tot}}$, which represent the fractions of K in the condensate at the start, at any time *t*, and at equilibrium, respectively, Eq. S24 takes the form,

$$f = f_e-(f_e-f_0)\,e^{-3\gamma_{\mathrm{K}}\sqrt{\frac{RT}{2\pi m_{\mathrm{K}}}}\frac{r^2}{\mathcal{R}^3}\frac{t}{f_e}}. \text{(S25)}$$

The equation gives the time evolution of the condensed K fraction. From this equation, we can also express t as a function of the condensed fraction f,

$$t = -\frac{f_e}{3\gamma_{\mathrm{K}}\sqrt{\frac{RT}{2\pi m_{\mathrm{K}}}}\frac{r^2}{\mathcal{R}^3}}\ln\frac{f_e-f}{f_e-f_0}. \text{(S26)}$$

We can apply Eq. S25 to isotopes *j* and *i*,

$$f_j = f_{e,j}-(f_{e,j}-f_{0,j})\,e^{-3\gamma_{\mathrm{K},j}\sqrt{\frac{RT}{2\pi m_{\mathrm{K},j}}}\frac{r^2}{\mathcal{R}^3}\frac{t}{f_{e,j}}}. \text{(S27)}$$
$$f_i = f_{e,i}-(f_{e,i}-f_{0,i})\,e^{-3\gamma_{\mathrm{K},i}\sqrt{\frac{RT}{2\pi m_{\mathrm{K},i}}}\frac{r^2}{\mathcal{R}^3}\frac{t}{f_{e,i}}}. \text{(S28)}$$

We are interested in the isotopic ratio in the condensate, which can be obtained by dividing Eq. S27 by Eq. S28,

$$\frac{n_{\mathrm{K},j}/n_{\mathrm{K},i}}{n_{\mathrm{K,tot},j}/n_{\mathrm{K,tot},i}} = \frac{f_j}{f_i} = \frac{f_{e,j}-(f_{e,j}-f_{0,j})\,e^{-3\gamma_{\mathrm{K},j}\sqrt{\frac{RT}{2\pi m_{\mathrm{K},j}}}\frac{r^2}{\mathcal{R}^3}\frac{t}{f_{e,j}}}}{f_{e,i}-(f_{e,i}-f_{0,i})\,e^{-3\gamma_{\mathrm{K},i}\sqrt{\frac{RT}{2\pi m_{\mathrm{K},i}}}\frac{r^2}{\mathcal{R}^3}\frac{t}{f_{e,i}}}}. \text{(S29)}$$

The left side of the equation is the isotopic ratio j/i in the condensate divided by that in the bulk. We can simplify the right side of the equation, by introducing the equilibrium isotopic fractionation factor (α) between the condensate and the vapor,

$$\alpha_e = \frac{n_{\mathrm{K},e,j}/n_{\mathrm{K},e,i}}{(n_{\mathrm{K,tot},j}-n_{\mathrm{K},e,j})/(n_{\mathrm{K,tot},i}-n_{\mathrm{K},e,i})} = \frac{f_{e,j}/f_{e,i}}{(1-f_{e,j})/(1-f_{e,i})}, \text{(S30)}$$
$$\alpha_0 = \frac{n_{\mathrm{K},0,j}/n_{\mathrm{K},0,i}}{(n_{\mathrm{K,tot},j}-n_{\mathrm{K},0,j})/(n_{\mathrm{K,tot},i}-n_{\mathrm{K},0,i})} = \frac{f_{0,j}/f_{0,i}}{(1-f_{0,j})/(1-f_{0,i})}. \text{(S31)}$$

We therefore have,

$$f_{e,j} = \frac{\alpha_e}{1-f_{e,i}+\alpha_e f_{e,i}} f_{e,i}. \text{ (S32)}$$
$$f_{0,j} = \frac{\alpha_0}{1-f_{0,i}+\alpha_0 f_{0,i}} f_{0,i}. \text{ (S33)}$$

To simplify the exponential terms in Eq. S29, we express them as a function $y(x)$, with $x = \gamma_{\mathrm{K}}/\sqrt{m_{\mathrm{K}}}$,

$$y(x) = e^{-3x\sqrt{\frac{RT}{2\pi}}\frac{r^2}{\mathcal{R}^3}\frac{t}{f_e}}. \text{ (S34)}$$

The difference between $\gamma_{\mathrm{K},j}/\sqrt{m_{\mathrm{K},j}}$ and $\gamma_{\mathrm{K},i}/\sqrt{m_{\mathrm{K},i}}$ is small as we are considering two isotopes of the same element with nearly the same mass. Therefore, we can use the following approximation,

$$y(x_j) \simeq y(x_i) + \frac{\partial y}{\partial x_i}(x_j - x_i), \text{ (S35)}$$

which translates to,

$$e^{-3\gamma_{\mathrm{K},j}\sqrt{\frac{RT}{2\pi m_{\mathrm{K},j}}}\frac{r^2}{\mathcal{R}^3}\frac{t}{f_{e,j}}} \simeq \left[1 - \sqrt{\frac{RT}{2\pi}}\frac{3r^2}{\mathcal{R}^3}\frac{t}{f_{e,i}}\left(\frac{\gamma_{\mathrm{K},j}}{\sqrt{m_{\mathrm{K},j}}} - \frac{\gamma_{\mathrm{K},i}}{\sqrt{m_{\mathrm{K},i}}}\right)\right] e^{-3\gamma_{\mathrm{K},i}\sqrt{\frac{RT}{2\pi m_{\mathrm{K},i}}}\frac{r^2}{\mathcal{R}^3}\frac{t}{f_{e,i}}}. \text{ (S36)}$$

If we introduce the kinetic isotopic fractionation factor α_{kin},

$$\alpha_{kin} = \frac{\gamma_{\mathrm{K},j}}{\sqrt{m_{\mathrm{K},j}}} / \frac{\gamma_{\mathrm{K},i}}{\sqrt{m_{\mathrm{K},i}}}, \text{ (S37)}$$

Eq. S36 can then be expressed as,

$$e^{-3\gamma_{\mathrm{K},j}\sqrt{\frac{RT}{2\pi m_{\mathrm{K},j}}}\frac{r^2}{\mathcal{R}^3}\frac{t}{f_{e,j}}} \simeq \left[1 - \sqrt{\frac{RT}{2\pi}}\frac{3r^2}{\mathcal{R}^3}\frac{t}{f_{e,i}}\frac{\gamma_{\mathrm{K},i}}{\sqrt{m_{\mathrm{K},i}}}(a_{kin} - 1)\right] e^{-3\gamma_{\mathrm{K},i}\sqrt{\frac{RT}{2\pi m_{\mathrm{K},i}}}\frac{r^2}{\mathcal{R}^3}\frac{t}{f_{e,i}}}. \text{ (S38)}$$

Introducing Eqs. S26, S32, S33, and S38 into Eq. S29, and using the following approximation ($\alpha_{kin} - 1$ is close to 0),

$$(\alpha_{kin} - 1)\, ln\frac{f_{e,i}-f_i}{f_{e,i}-f_{0,i}} \simeq \left(\frac{f_{e,i}-f_i}{f_{e,i}-f_{0,i}}\right)^{(\alpha_{kin}-1)} - 1, \text{ (S39)}$$

Eq. S29 can be simplified as,

$$\frac{n_{\mathrm{K},j}/n_{\mathrm{K},i}}{n_{\mathrm{K,tot},j}/n_{\mathrm{K,tot},i}} = \frac{\alpha_e f_e}{f(1+\alpha_e f_e - f_e)} + \left[\frac{\alpha_0 f_0}{f(1-f_0+\alpha_0 f_0)} - \frac{\alpha_e f_e}{f(1+\alpha_e f_e - f_e)}\right]\left(\frac{f_e - f}{f_e - f_0}\right)^{\alpha_{kin}}. \text{ (S40)}$$

The isotopic composition of the condensate δ_c (relative to the bulk) as a function of the condensed fraction f then takes the form,

$$\delta_c = 1000 \ln\left\{\frac{\alpha_e f_e}{f(1+\alpha_e f_e - f_e)} + \left(\frac{\alpha_0 f_0}{f(1+\alpha_0 f_0 - f_0)} - \frac{\alpha_e f_e}{f(1+\alpha_e f_e - f_e)}\right)\left(\frac{f_e - f}{f_e - f_0}\right)^{\alpha_{kin}}\right\}. \text{ (S41)}$$

Using the fact that $\alpha_0 \simeq 1$, $\alpha_e \simeq 1$, and $\alpha_{kin} \simeq 1$, one can show that Eq. S41 can be approximated as,

$$\delta_c = \frac{(1-f_e)f_e(f-f_0)}{f(f_e-f_0)}\Delta_e + \frac{(f-f_e)f_0(f_0-1)}{f(f_e-f_0)}\Delta_0 + \frac{(f-f_e)}{f}\ln\left(\frac{f_e-f}{f_e-f_0}\right)\Delta_{kin}, \text{ (S42)}$$

where Δ is isotopic fractionation in ‰ defined as $\Delta = 1000\,(\alpha - 1)$.

δ_c (*i.e.*, Eq. S42) can also be expressed as a function of time by simply replacing f with the expression that gives its time evolution (Eq. S25).

Below, we validate our numerical simulations against the formula that we have derived for instantaneous cooling. In our numerical model, we simulate instantaneous cooling by equilibrating chondrule melt and vapor at an initial temperature T_0 of 1823 K, and then setting a lower temperature for the system to evolve to equilibrium. At the initial temperature, with the assumed radius of the chondrule (r = 0.5 mm) and the preferred radius of the surrounding gas parcel ($\mathcal{R}$ = 0.069 m), about 0.24×CI K is in the melt and 0.76×CI K in the vapor (*i.e.*, f_0 = 0.24). Isotopic fractionation factors are assumed to be $\alpha_{kin} = \sqrt{m_{^{39}\mathrm{K}}/m_{^{41}\mathrm{K}}}$, and $\alpha_0 = \alpha_e = 1$. We calculate the evolution trajectories for various final temperatures, corresponding to different fractions of the element in the melt at final equilibrium. In Fig. S2, we show the cooling trajectories for five temperature drops (final temperature T_e ranging from 1773 K to 1323 K). The plots show the time evolution of the condensed fraction f (Fig. S2A) and the isotopic fractionation of the condensate δ_c (Fig. S2B), as well as δ_c against f (Fig. S2C). We also plot on the figure the results from our analytical equations (Eqs. S42 and S25). As shown in Fig. S2, the curves obtained using the numerical model (solid lines) agree with the analytical equations (open symbols), which validates the numerical model. The curves show that as the degree of undercooling $\Delta T = T_e - T_0$ gets higher, the fraction of K condensed and the maximum isotopic fractionation produced are larger, as is expected.

<u>Radius of the chondrule ambient gas ($\mathcal{R}$) and average chondrule cooling rate</u>

As discussed above, the value of $\mathcal{R}$ is determined by the fraction of K in the chondrule melt (f_{K}) at the peak temperature of 1823 K (Eq. S16). Because equilibrium is assumed at peak temperature, the value of $\mathcal{R}$ does not depend on the cooling rate. Different $\mathcal{R}$ values would, however, lead to different cooling rates, and different elemental and isotopic trajectories. The fraction of K in chondrule at peak temperature is not precisely known, but previous work showed that most likely chondrules did not lose all their MVEs during heating. A study of Na content in olivine phenocrysts in type I and II chondrules concluded that significant amount of Na was present when olivine was crystalizing (*48*). Another study of Na abundance in melt inclusions in olivine and chondrule glasses in type II chondrules showed that melt inclusions in olivine had Na amount lower than

expected from crystal-liquid elemental fractionation relative to chondrule glass (*49*). According to (*49*), chondrules could have evaporated ~50% or more of their total condensed Na before re-condensation.

These studies are mainly based on type II chondrules in ordinary chondrites. In carbonaceous chondrites, type I chondrules dominate, and they are more depleted in MVEs (*87*). Type II chondrules have inventories of Na and K close to CI, but type I chondrules have K abundance of ~0.48×CI (Table S1). For lack of better constraints, we assume that similar to type II chondrules, type I chondrules retained about 50 % (*i.e.*, ~0.24×CI) of their final inventory of K (*i.e.*, ~0.48×CI) at peak temperature. In other words, at peak temperature, 0.24×CI K is in the chondrule melt and 0.76×CI K is in the gas. Another ~0.24×CI K then condenses from the gas into the chondrule melt during cooling, making up a total of ~0.48×CI K in the chondrule component. The $\mathcal{R}$ value and the cooling rate constrained based on this assumption are 0.069 m (Fig. S3; corresponding to a number density of 727 chondrule/m) and ~560±180 K/hr (Fig. 4), respectively.

Given uncertainties in the fraction of K in type I chondrule melt at peak temperature, we also calculated two extreme conditions, one with chondrules retaining 0.048×CI K (*i.e.*, only 10 % of their current K content) at peak temperature, and the other with chondrules retaining 0.43×CI K (*i.e.*, 90 % of their current K content) at peak temperature. In the two scenarios, the $\mathcal{R}$ values are calculated to be 0.127 m and 0.052 m, respectively, and the corresponding chondrule number densities are ~117 chondrule/m^3 and ~1698 chondrule/m^3. The calculated average chondrule cooling rates for these two scenarios are ~80±25 K/hr and ~1500±450 K/hr, respectively (Fig. S4). These cooling rate estimates based on Rb and K isotopes are consistent with the cooling rates (10–1000 K/hr) constrained from laboratory experiments aimed at reproducing chondrule textures (*e.g.*, (*66–68*) and references therein).

Cooling rates recorded by individual chondrules

The elemental and isotopic compositions of the calculated chondrule component represent averages. Individual chondrules have variable compositions and they might have experienced different thermal histories. Jiang *et al*. (*22*) measured the isotopic compositions of K in individual bulk chondrules from Allende. A difficulty with interpreting single chondrule data is that the isotopic compositions of individual chondrules may have been modified by parent-body aqueous alteration and metamorphism. In Allende, fine-grained refractory inclusions, which presumably did not incorporate any Na or K when they formed at high temperature in the nebula, are now full of Na-rich aqueous alteration products such as nepheline and sodalite (*32*), demonstrating that Na was extensively mobilized by fluids on the Allende parent body. A second complication is that sample selection might have been biased towards larger chondrules as small chondrules would be challenging to separate and analyze. With these caveats in mind, we can use the same modeling approach as that used for our chondrule component to calculate the cooling rates of the individual chondrules measured in (*22*).

In Table S2, we report the calculated cooling rates of individual chondrules. The isotopic compositions of individual chondrules relative to CI-like matrix ($\Delta^{41}K_{Chondrule\text{-}CI}$) were obtained by subtracting the $\delta^{41}K$ value of CI-like matrix constrained in this study (0.04±0.08 ‰) from that of the individual chondrules reported in (*22*). The isotopic compositions (relative to CI-like matrix) range from −0.28 to −0.91 ‰, with a weighted bulk of −0.39±0.05 ‰ (weighted by chondrule size

and K content), similar to that of our calculated chondrule component (−0.37±0.15 ‰; Table S1). The degrees of K depletion in the chondrules were quantified using K/Al ratios (*22*) normalized to that of CI chondrites (0.0651; (*88*)). To calculate cooling rates, the radii of the chondrule (r) and of the surrounding gas ($\mathcal{R}$) are needed. The chondrule radii were calculated using the reported chondrule weights (*22*) by assuming a density of 3.15 g cm^{-3} (*82*). We further assume a constant $\mathcal{R}/r$ ratio, meaning that at large scale, the chondrule-gas cloud had a homogeneous density of condensable mass. For lack of better constraints, we anchor this ratio to the values that we used to calculate the condensation trajectories of the chondrule component (Figs. 4 and S4). We considered two $\mathcal{R}/r$ ratios ($\mathcal{R}/r$ = 254 and 138; Table S2) in our calculation, corresponding to 0.048×CI and 0.24×CI K in the chondrule component at peak temperature, respectively.

Assuming a constant $\mathcal{R}/r$ ratio results in the same amount of K relative to CI present in the chondrule melt at peak temperature (1823 K; the starting point of the simulation) for all chondrules (~0.048×CI for $\mathcal{R}/r$ = 254 and 0.24×CI for $\mathcal{R}/r$ = 138). No cooling rate was obtained for chondrule #13 from (*22*) because its total K amount is only 0.03×CI (Table S2), which is less than the calculated initial amount of 0.048×CI. For $\mathcal{R}/\mathrm{r}$ = 254, the calculated cooling rates of individual chondrules range from 50 to 400 K/hr (except for chondrule #13). For the lower $\mathcal{R}/\mathrm{r}$ ratio of 138, cooling rates were obtained for 11 out of 17 chondrules, with values ranging from 400–2300 K/hr. The cooling rates inferred for these chondrules are overall in agreement with estimates based on chondrule textures (~10–1000 K/hr; *e.g.*, (*66–68*) and references therein). However, as discussed above, the K inventories and isotopic compositions of chondrules in Allende may have been affected by parent-body processing.

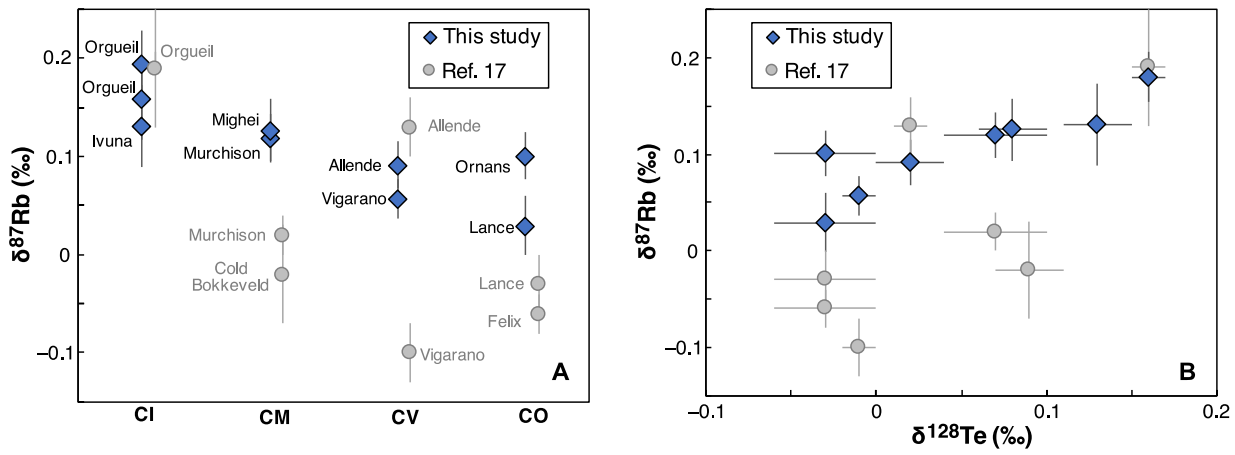

Fig. S1.

Rubidium isotopic compositions measured in this study compared with previously published data (*17*). Discrepancies are found for Murchison and Vigarano (panel A). We used two different chromatography methods to test the accuracy of our Rb data and found very consistent results (see Methods). When plotting against Te isotopic compositions in (*23*), our Rb data show a trend with Te, which was not clear in previously published data (panel B).

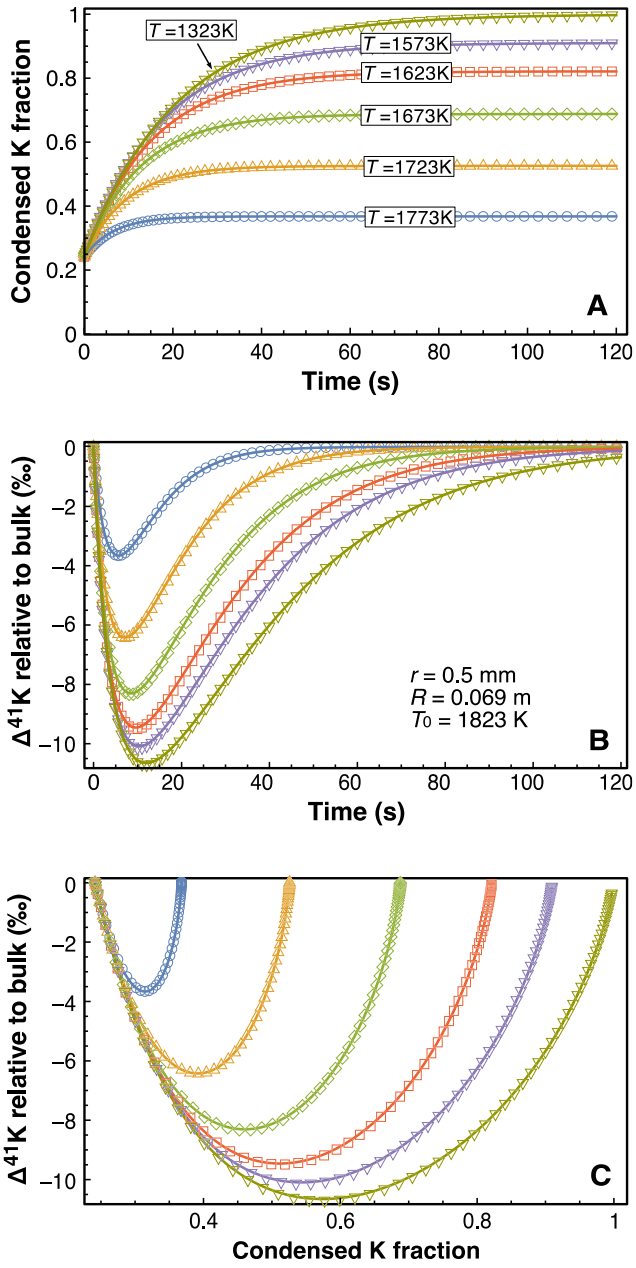

Fig. S2.

Modeled composition of the liquid condensate during instantaneous cooling, calculated by assuming initial equilibrium at 1823 K between liquid and vapor (concentric spheres with radii of 0.5 mm and 0.069 m, respectively), and instantaneously decreasing the temperature so that the vapor becomes supersaturated. The curves are labelled with the final temperatures. The solid lines were calculated using our numerical model (Eqs. S12 and S14), while the open symbols were calculated using the analytical equations derived in the Supplement (Eqs. S25 and S42). As shown, the two modeling approaches agree, which validates our numerical code for calculating isotopic fractionation during condensation for finite cooling rates.

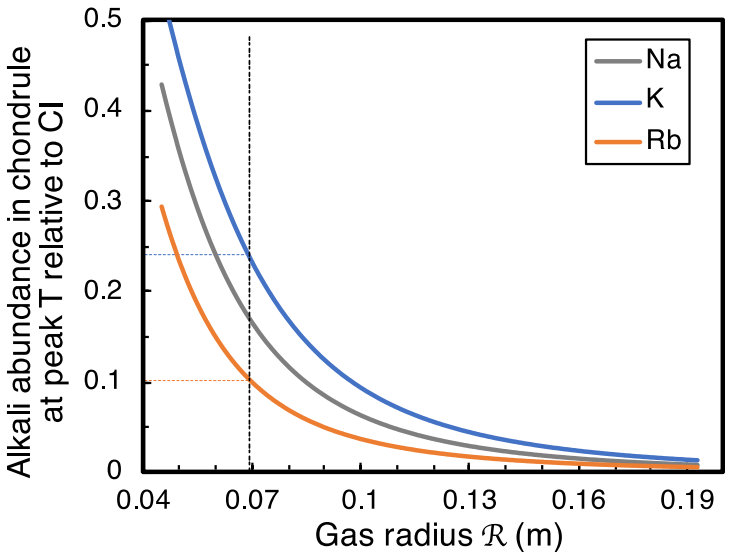

Fig. S3.

Fraction of alkali elements in chondrule melt (as opposed to ambient gas) at assumed peak temperature (1823 K) as a function of the radius $\mathcal{R}$ of the gas parcel surrounding a 0.5 mm-radius chondrule. Equilibrium between the chondrule melt and the gas is assumed. The K and Rb amount in the chondrule component (*i.e.*, the total condensed amount) are 0.48×CI and 0.43×CI respectively (Table S1). Assuming that 0.24×CI K (*i.e.*, half of the total K in the chondrule component; blue dashed line) remained in the chondrule melt at peak temperature, the gas radius $\mathcal{R}$ surrounding the chondrule droplet would be 0.069 m (black dashed line), and the corresponding Rb amount in the chondrule melt at the temperature would be ~0.1×CI (orange dashed line).

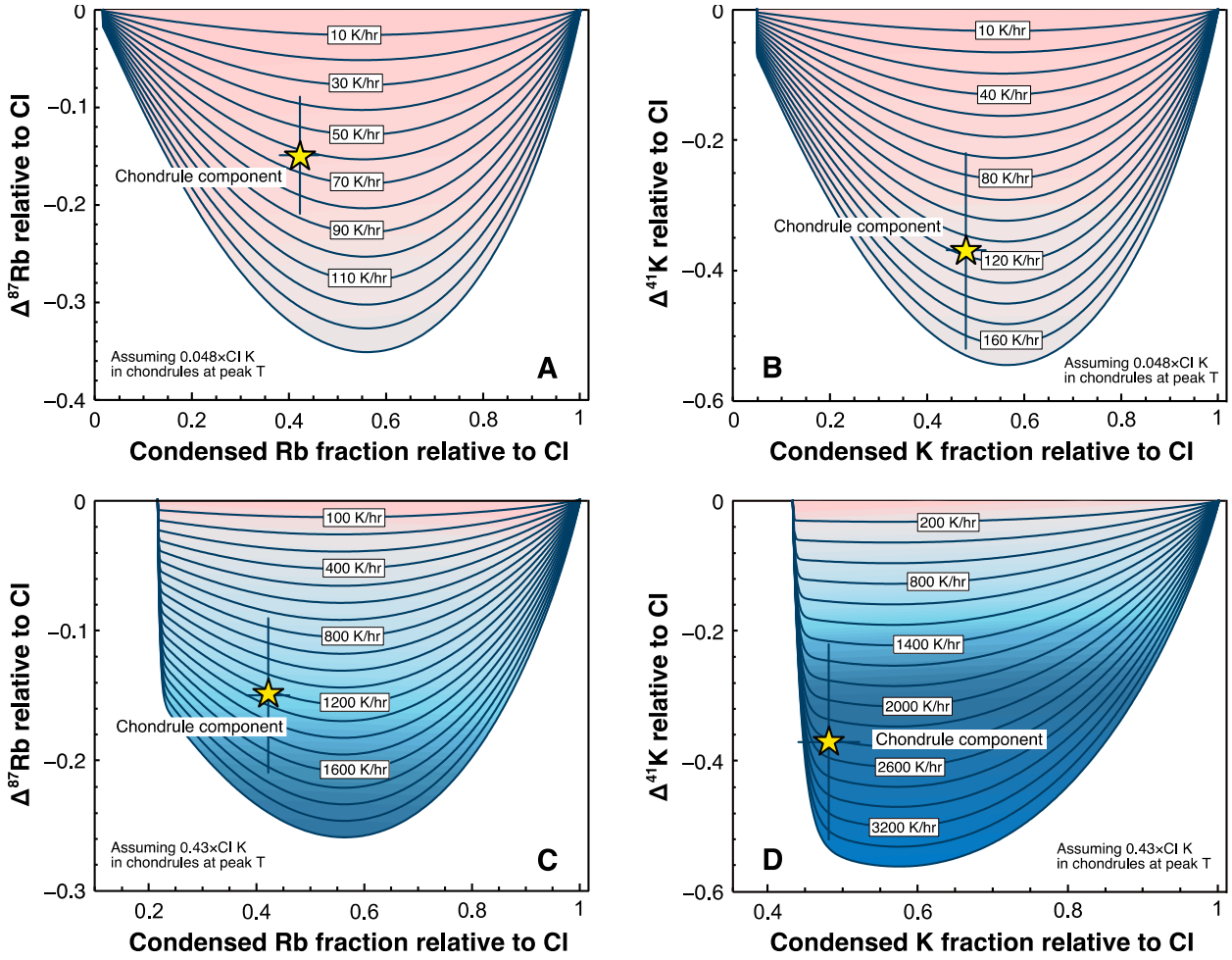

Fig. S4.

Modeled trajectories of Rb and K isotopic fractionations against their condensed fractions during chondrule cooling. The chondrule was set to have a radius of 0.5 mm. Two scenarios with different gas radii $\mathcal{R}$ are considered: panels A and B assume that 0.048×CI K is present in the chondrule melt at the peak temperature of 1823 K (corresponding to $\mathcal{R}$ = 0.127 m; Fig. S3), and panels C and D assume that 0.43×CI K is present in the chondrule melt at the peak temperature (corresponding to $\mathcal{R}$ = 0.052 m; Fig. S3). The Rb and K compositions of the chondrule component (yellow stars) give consistent cooling rates within error for each scenario, and the cooling rates are 80±25 K/hr (weighted mean of cooling rates from K and Rb) in the first scenario and 1500±450 K/hr in the second scenario.

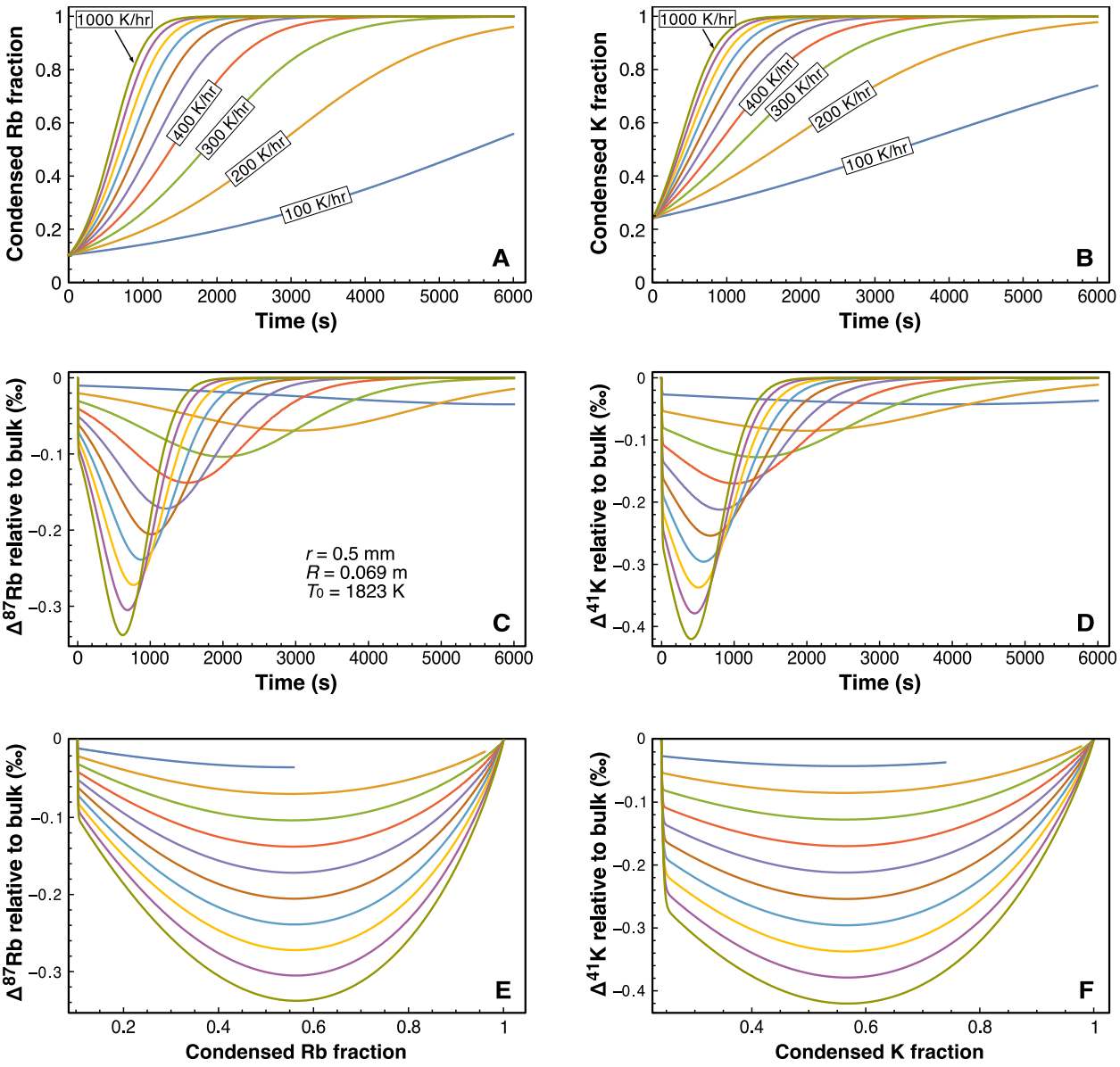

Fig. S5.

Modeled trajectories of chondrule melt composition during cooling under finite cooling rates. The calculation was done by assuming an initial temperature of 1823 K, and adopting radii for the chondrule and surrounding vapor of 0.5 mm and 0.069 m, respectively. Panels A, C, and E are for Rb condensation, while panels B, D, and F are for K condensation.

Table S1.

Average Rb, K, Te, and Zn elemental and isotopic compositions of the CC groups and the calculated chondrule and matrix components.

	Matrix mass fraction*	Rb (μg/g)	K (μg/g)	Te (μg/g)	Zn (μg/g)	δ^{87}Rb ± 2σ (‰)‡	δ^{41}K ± 2σ (‰)‡	δ^{128}Te ± 2SD (‰)	δ^{66}Zn ± 2SD (‰)
CI	1	2.3†	546†	2.29±0.10*	309†	0.17±0.02	−0.07±0.61§ (−0.20±0.57)§	0.15±0.04*	0.46±0.10‖
CM	0.41±0.12	1.7†	403†	1.43±0.15*	180†	0.12±0.02	−0.12±0.35	0.08±0.02*	0.38±0.04‖
CV	0.30±0.07	1.3†	310†	0.90±0.13*	107†	0.07±0.21	−0.27±0.92	0.01±0.02*	0.24±0.12‖
CO	0.20±0.12	1.5†	345†	0.82±0.03*	100†	0.07±0.44	−0.15±1.19	−0.03±0.03*	0.17±0.11‖
CR	0.09±0.05	1.1†	303†	0.49±0.03*	96†				
Tagish Lake	0.64±0.23	1.8†	334†	1.67±0.04*	216†				
CI-like matrix¶	1	2.37±0.15	535.7±35.9	2.31±0.10	307.3±19.8	0.19±0.03	0.04±0.08	0.15±0.01	0.47±0.03
Chondrule component¶	0	1.00±0.06	259.7±14.3	0.34±0.05	59.6±7.4	0.04±0.05	−0.33±0.12	−0.38±0.09	0.05±0.09
Abundance in chondrule relative to matrix		0.42±0.04 CI	0.48±0.04 CI	0.15±0.02 CI	0.19±0.03 CI				
Isotope fractionation ($\Delta_{chondrule-matrix}$)						−0.15±0.06	−0.37±0.15	−0.53±0.10	−0.42±0.10

*Matrix mass fractions, Te concentrations and isotopic compositions are from (*23*, *89*–*95*). †Rubidium, K, and Zn concentrations of CC groups are from (*26*), and a ±10% error was assumed for these concentrations when calculating the elemental composition of the chondrule component by linear regression (Fig. 2). ‡Group means and errors of Rb and K isotopic compositions are calculated as weighted means and 95% c.i. using Isoplot. §The average CI δ^{41}K value is −0.07±0.61 when Ivuna is excluded and is −0.20±0.57 when Ivuna is included. ‖Zinc isotopic compositions are taken from (*24*, *25*). ¶The elemental and isotopic compositions of the CI-like matrix and the chondrule component are calculated using the linear regressions in Fig. 2.

Table S2.
Calculated cooling rates of individual chondrules.

No.*	Chond. wt. (mg)*	Chond. radius r (mm)†	$(K/Al)_{CI}$ wt. ratio‡	$\Delta^{41}K_{Chond.-CI}$§	Assumed total K (×CI)‖	Gas radius $\mathcal{R}$ (m) ($\mathcal{R}/r$=254)¶	Cooling rate (K/hr)#	Gas radius $\mathcal{R}$ (m) ($\mathcal{R}/r$=138)¶	Cooling rate (K/hr)#
CH1	8.22	0.854	0.507	−0.28±0.09	1	0.217	51±18	0.118	390±120
CH2	12.9	0.992	0.123	−0.31±0.08	1	0.252	145±40	0.137	/
CH3	18.67	1.123	0.276	−0.38±0.08	1	0.285	75±15	0.155	580±120
CH4	9.47	0.895	0.184	−0.28±0.09	1	0.227	100±30	0.124	/
CH5	4.58	0.703	0.476	−0.34±0.08	1	0.179	78±20	0.097	600±150
CH6	2.36	0.563	0.154	−0.42±0.11	1	0.143	280±80	0.078	/
CH7	1.51	0.486	0.630	−0.33±0.10	1	0.123	110±30	0.067	820±240
CH8	4.26	0.686	0.307	−0.38±0.14	1	0.174	112±45	0.095	880±320
CH9	4.62	0.705	0.276	−0.45±0.08	1	0.179	140±25	0.097	1120±200
CH10	3.79	0.660	0.108	−0.48±0.09	1	0.168	400±100	0.091	/
CH11	8.92	0.878	0.276	−0.31±0.09	1	0.223	78±25	0.121	600±180
CH12	2.32	0.560	0.430	−0.91±0.11	1	0.142	280±40	0.077	2200±300
CH13	13.83	1.016	0.030	−0.84±0.08	1	0.258	/	0.140	/
CH14	44.59	1.501	0.215	−0.44±0.14	1	0.381	80±25	0.207	/
CH15	1.06	0.431	0.430	−0.41±0.10	1	0.110	155±35	0.060	1200±300
CH16	0.35	0.298	0.430	−0.53±0.11	1	0.076	300±170	0.041	2300±600
CH17	0.67	0.370	0.430	−0.32±0.09	1	0.094	140±40	0.051	1100±300

*Chondrule no. and chondrule weights are from Jiang *et al.* (*22*). †Chondrule radius is calculated using the chondrule weights and an assumed density of 3.15 g cm^{-3} (*82*). ‡K/Al weight ratio relative to CI is calculated by dividing the K/Al weight ratio reported in (*22*) by 0.0651 (*i.e.*, the K/Al weight ratio of CI chondrites; (*88*)). §Isotopic differences between chondrules and CI-like matrix ($\Delta^{41}K_{Chond.-CI}$) are calculated by subtracting the K isotopic composition of CI-like matrix (0.04±0.08 ‰; Table S1) from the measured K isotopic compositions of individual chondrules reported in (*22*). ‖The bulk gas-chondrule is assumed to have CI-like K amount. ¶Gas radius is calculated by assuming a constant mass density of condensable matter, *i.e.*, a constant $\mathcal{R}/r$ ratio for all chondrules. Two $\mathcal{R}/r$ ratios that were used for calculating the cooling rate of the chondrule component were applied here. The first one ($\mathcal{R}/r$=254) corresponds to 0.048×CI K in the chondrule component at the peak T of 1823K; Fig. S4), while the second one ($\mathcal{R}/r$=138) corresponds to 0.24×CI K in the chondrule component at the peak T (Fig. 4). #Cooling rates were not obtained for chondrules that have total K amount less than the calculated K amount in the molten chondrule at peak T, which is determined by the $\mathcal{R}/r$ ratio.

REFERENCES AND NOTES

1. E. R. D. Scott, A. N. Krot, Chondrites and their components, in *Meteorites and Cosmochemical Processes*, A. M. Davis, Ed. (Elsevier, Oxford, 2014), vol. 1, pp. 65–137.

2. R. N. Clayton, Oxygen isotopes in meteorites. *Annu. Rev. Earth Planet. Sci.* **21**, 115–149 (1993).

3. N. Dauphas, The isotopic nature of the Earth's accreting material through time. *Nature* **541**, 521–524 (2017).

4. A. M. Davis, Volatile evolution and loss, in *Meteorites and the Early Solar System II*, D. S. Lauretta and H. Y. McSween Jr., Eds. (University of Arizona Press, 2006), pp. 295–307.

. F. M. Richter, A. M. Davis, D. S. Ebel, A. Hashimoto, Elemental and isotopic fractionation of Type B calcium-, aluminum-rich inclusions: Experiments, theoretical considerations, and constraints on their thermal evolution. *Geochim. Cosmochim. Acta* **66**, 521–540 (2002).

6. F. M. Richter, P. E. Janney, R. A. Mendybaev, A. M. Davis, M. Wadhwa, Elemental and isotopic fractionation of Type B CAI-like liquids by evaporation. *Geochim. Cosmochim. Acta* **71**, 5544–5564 (2007).

7. F. M. Richter, Timescales determining the degree of kinetic isotope fractionation by evaporation and condensation. *Geochim. Cosmochim. Acta* **68**, 4971–4992 (2004).

8. N. Dauphas, F. Poitrasson, C. Burkhardt, H. Kobayashi, K. Kurosawa, Planetary and meteoritic Mg/Si and δ^{30} Si variations inherited from solar nebula chemistry. *Earth Planet. Sci. Lett.* **427**, 236–248 (2015).

9. K. Lodders, Solar system abundances and condensation temperatures of the elements. *Astrophys. J.* **591**, 1220–1247 (2003).

10. F.-Z. Teng, N. Dauphas, J. M. Watkins, Non-traditional stable isotopes: Retrospective and prospective. *Rev. Mineral. Geochem.* **82**, 1–26 (2017).

11. C. M. O. Alexander, J. N. Grossman, J. Wang, B. Zanda, M. Bourot-Denise, R. H. Hewins, The lack of potassium-isotopic fractionation in Bishunpur chondrules. *Meteorit. Planet. Sci*. **35**, 859–868 (2000).

12. C. M. O. Alexander, J. N. Grossman, Alkali elemental and potassium isotopic compositions of Semarkona chondrules. *Meteorit. Planet. Sci*. **40**, 541–556 (2005).

13. K. Wang, S. B. Jacobsen, Potassium isotopic evidence for a high-energy giant impact origin of the Moon. *Nature* **538**, 487–490 (2016).

14. Z. Tian, H. Chen, B. Fegley, K. Lodders, J.-A. Barrat, J. M. D. Day, K. Wang, Potassium isotopic compositions of howardite-eucrite-diogenite meteorites. *Geochim. Cosmochim. Acta* **266**, 611–632 (2019).

15. Z. Tian, B. L. Jolliff, R. L. Korotev, B. Fegley, K. Lodders, J. M. D. Day, H. Chen, K. Wang, Potassium isotopic composition of the Moon. *Geochim. Cosmochim. Acta* **280**, 263–280 (2020).

16. H. Bloom, K. Lodders, H. Chen, C. Zhao, Z. Tian, P. Koefoed, M. K. Pető, Y. Jiang, K. Wang, Potassium isotope compositions of carbonaceous and ordinary chondrites: Implications on the origin of volatile depletion in the early solar system. *Geochim. Cosmochim. Acta* **277**, 111–131 (2020).

17. E. A. Pringle, F. Moynier, Rubidium isotopic composition of the Earth, meteorites, and the Moon: Evidence for the origin of volatile loss during planetary accretion. *Earth Planet. Sci. Lett.* **473**, 62–70 (2017).

18. N. X. Nie, N. Dauphas, Vapor drainage in the protolunar disk as the cause for the depletion in volatile elements of the moon. *Astrophys. J. Lett.* **884**, L48 (2019).

19. Y. Ku, S. B. Jacobsen, Potassium isotope anomalies in meteorites inherited from the protosolar molecular cloud. *Sci. Adv.* **6**, eabd0511 (2020).

0. P. Koefoed, O. Pravdivtseva, H. Chen, C. Gerritzen, M. M. Thiemens, K. Wang, Potassium isotope systematics of the LL4 chondrite Hamlet: Implications for chondrule formation and alteration. *Meteorit. Planet. Sci*. **55** (2020).

21. C. Zhao, K. Lodders, H. Bloom, H. Chen, Z. Tian, P. Koefoed, M. K. Pető, K. Wang, Potassium isotopic compositions of enstatite meteorites. *Meteorit. Planet. Sci*. **55**, 1404–1417 (2020).

22. Y. Jiang, P. Koefoed, O. Pravdivtseva, H. Chen, C.-H. Li, F. Huang, L.-P. Qin, J. Liu, K. Wang, Early solar system aqueous activity: K isotope evidence from Allende. *Meteorit. Planet. Sci*. **56**, 61–76 (2021).

23. J. L. Hellmann, T. Hopp, C. Burkhardt, T. Kleine, Origin of volatile element depletion among carbonaceous chondrites. *Earth Planet. Sci. Lett.* **549**, 116508 (2020).

24. J.-M. Luck, D. B. Othman, F. Albarède, Zn and Cu isotopic variations in chondrites and iron meteorites: Early solar nebula reservoirs and parent-body processes. *Geochim. Cosmochim. Acta* **69**, 5351–5363 (2005).

25. E. A. Pringle, F. Moynier, P. Beck, R. Paniello, D. C. Hezel, The origin of volatile element depletion in early solar system material: Clues from Zn isotopes in chondrules. *Earth Planet. Sci. Lett.* **468**, 62–71 (2017).

26. C. M. O. Alexander, Quantitative models for the elemental and isotopic fractionations in chondrites: The carbonaceous chondrites. *Geochim. Cosmochim. Acta* **254**, 277–309 (2019).

27. D. Clayton, *Handbook of Isotopes in the Cosmos: Hydrogen to Gallium* (Cambridge Univ. Press, 2007).

28. E. Anders, N. Grevesse, Abundances of the elements: Meteoritic and solar. *Geochim. Cosmochim. Acta* **53**, 197–214 (1989).

29. Y. Hu, X.-Y. Chen, Y.-K. Xu, F.-Z. Teng, High-precision analysis of potassium isotopes by HR-MC-ICPMS. *Chem. Geol.* **493**, 100–108 (2018).

30. M. A. Fehr, S. J. Hammond, I. J. Parkinson, Tellurium stable isotope fractionation in chondritic meteorites and some terrestrial samples. *Geochim. Cosmochim. Acta* **222**, 17–33 (2018).

31. A. N. Krot, E. R. D. Scott, M. E. Zolensky, Mineralogical and chemical modification of components in CV3 chondrites: Nebular or asteroidal processing? *Meteoritics* **30**, 748–775 (1995).

32. A. Hashimoto, L. Grossman, Alteration of Al-rich inclusions inside amoeboid olivine aggregates in the Allende meteorite. *Geochim. Cosmochim. Acta* **51**, 1685–1704 (1987).

33. E. Anders, Origin, age, and composition of meteorites. *Space Sci. Rev*. **3**, 583–714 (1964).

34. J. W. Larimer, E. Anders, Chemical fractionations in meteorites—II. Abundance patterns and their interpretation. *Geochim. Cosmochim. Acta* **31**, 1239–1270 (1967).

35. F. Wlotzka, H. Palme, B. Spettel, H. Wänke, K. Fredriksson, A. F. Noonan, Alkali differentiation in LL-chondrites. *Geochim. Cosmochim. Acta* **47**, 743–757 (1983).

6. T. Yokoyama, K. Misawa, O. Okano, C.-Y. Shih, L. E. Nyquist, J. I. Simon, M. J. Tappa, S. Yoneda, Extreme early solar system chemical fractionation recorded by alkali-rich clasts contained in ordinary chondrite breccias. *Earth Planet. Sci. Lett.* **458**, 233–240 (2017).

37. L. H. Fuchs, Djerfisherite, alkali copper-iron sulfide: A new mineral from enstatite chondrites. *Science* **153**, 166–167 (1966).

8. J. L. Hellmann, T. Hopp, C. Burkhardt, H. Becker, M. Fischer-Gödde, T. Kleine, Tellurium isotope cosmochemistry: Implications for volatile fractionation in chondrite parent bodies and origin of the late veneer. *Geochim. Cosmochim. Acta* **309**, 313–328 (2021).

39. F. Wombacher, M. Rehkämper, K. Mezger, A. Bischoff, C. Münker, Cadmium stable isotope cosmochemistry. *Geochim. Cosmochim. Acta* **72**, 646–667 (2008).

40. M. Schönbächler, R. W. Carlson, M. F. Horan, T. D. Mock, E. H. Hauri, Silver isotope variations in chondrites: Volatile depletion and the initial 107Pd abundance of the solar system. *Geochim. Cosmochim. Acta* **72**, 5330–5341 (2008).

41. H. Palme, D. C. Hezel, D. S. Ebel, The origin of chondrules: Constraints from matrix composition and matrix-chondrule complementarity. *Earth Planet. Sci. Lett.* **411**, 11–19 (2015).

42. D. C. Hezel, H. Palme, The chemical relationship between chondrules and matrix and the chondrule matrix complementarity. *Earth Planet. Sci. Lett.* **294**, 85–93 (2010).

43. B. Zanda, M. Humayun, R. Hewins, Chemical composition of matrix and chondrules in carbonaceous chondrites: Implications for disk transport, in *Proceedings of the 43rd Annual Lunar and Planetary Science Conference*, Woodlands, TX, USA (19 to 23 March 2012), p. 2413.

44. E. M. M. E. van Kooten, F. Moynier, A. Agranier, A unifying model for the accretion of chondrules and matrix. *Proc. Natl. Acad. Sci. U.S.A.* **116**, 18860–18866 (2019).

45. E. van Kooten, F. Moynier, Zinc isotope analyses of singularly small samples (<5 ng Zn): Investigating chondrule-matrix complementarity in Leoville. *Geochim. Cosmochim. Acta* **261**, 248–268 (2019).

46. G. Libourel, A. N. Krot, L. Tissandier, Role of gas-melt interaction during chondrule formation. *Earth Planet. Sci. Lett.* **251**, 232–240 (2006).

47. G. Libourel, M. Portail, Chondrules as direct thermochemical sensors of solar protoplanetary disk gas. *Sci. Adv.* **4**, eaar3321 (2018).

48. C. M. O. Alexander, J. N. Grossman, D. S. Ebel, F. J. Ciesla, The formation conditions of chondrules and chondrites. *Science* **320**, 1617–1619 (2008).

49. R. H. Hewins, B. Zanda, C. Bendersky, Evaporation and recondensation of sodium in Semarkona Type II chondrules. *Geochim. Cosmochim. Acta* **78**, 1–17 (2012).

0. L. Florentin, F. Faure, E. Deloule, L. Tissandier, A. Gurenko, D. Lequin, Origin of Na in glass inclusions hosted in olivine from Allende CV3 and Jbilet Winselwan CM2: Implications for chondrule formation. *Earth Planet. Sci. Lett.* **474**, 160–171 (2017).

51. G. Libourel, A. Krot, L. Tissandier, Evidence for high temperature condensation of moderately-volatile elements during chondrule formation, in *Proceedings of the 34th Annual Lunar and Planetary Science Conference*, League City, TX, USA (17 to 21 March 2003), p. 1558.

52. R. D. Lewis, G. E. Lofgren, H. F. Franzen, K. E. Windom, The effect of Na vapor on the Na content of chondrules. *Meteoritics* **28**, 622–628 (1993).

53. B. A. Cohen, R. H. Hewins, C. M. O. Alexander, The formation of chondrules by open-system melting of nebular condensates. *Geochim. Cosmochim. Acta* **68**, 1661–1675 (2004).

54. F. M. Richter, R. A. Mendybaev, J. N. Christensen, D. Ebel, A. Gaffney, Laboratory experiments bearing on the origin and evolution of olivine-rich chondrules. *Meteorit. Planet. Sci*. **46**, 1152–1178 (2011).

55. A. V. Fedkin, L. Grossman, Vapor saturation of sodium: Key to unlocking the origin of chondrules. *Geochim. Cosmochim. Acta* **112**, 226–250 (2013).

56. P. Georges, G. Libourel, E. Deloule, Experimental constraints on alkali condensation in chondrule formation. *Meteorit. Planet. Sci*. **35**, 1183–1188 (2000).

57. H. Zeng, V. F. Rozsa, N. X. Nie, Z. Zhang, T. A. Pham, G. Galli, N. Dauphas, Ab initio calculation of equilibrium isotopic fractionations of potassium and rubidium in minerals and water. *ACS Earth Space Chem.* **3**, 2601–2612 (2019).

58. J. Y. Hu, N. Dauphas, F. L. H. Tissot, R. Yokochi, T. J. Ireland, Z. Zhang, A. M. Davis, F. J. Ciesla, L. Grossman, B. L. A. Charlier, M. Roskosz, E. E. Alp, M. Y. Hu, J. Zhao, Heating events in the nascent solar system recorded by rare earth element isotopic fractionation in refractory inclusions. *Sci. Adv.* **7**, eabc2962 (2021).

59. Y. Yu, R. H. Hewins, C. M. O. Alexander, J. Wang, Experimental study of evaporation and isotopic mass fractionation of potassium in silicate melts. *Geochim. Cosmochim. Acta* **67**, 773–786 (2003).

60. A. V. Fedkin, L. Grossman, M. S. Ghiorso, Vapor pressures and evaporation coefficients for melts of ferromagnesian chondrule-like compositions. *Geochim. Cosmochim. Acta* **70**, 206–223 (2006).

61. P. A. Sossi, S. Klemme, H. St. C. O'Neill, J. Berndt, F. Moynier, Evaporation of moderately volatile elements from silicate melts: Experiments and theory. *Geochim. Cosmochim. Acta* **260**, 204–231 (2019).

62. Z. J. Zhang, N. X. Nie, R. A. Mendybaev, M.-C. Liu, J. J. Hu, T. Hopp, E. E. Alp, B. Lavina, E. S. Bullock, K. D. McKeegan, Loss and isotopic fractionation of alkali elements during diffusion-limited evaporation from molten silicate: Theory and experiments. *ACS Earth Space Chem.* **5**, 755–784 (2021).

63. R. H. Hewins, H. C. Connolly Jr., Peak temperatures of flash-melted chondrules, in *Proceedings of the International conference: Chondrules and the Protoplanetary Disk* (1996), pp. 197–204.

64. R. H. Hewins, P. M. Radomsky, Temperature conditions for chondrule formation. *Meteoritics* **25**, 309–318 (1990).

65. F. M. Richter, N. Dauphas, F.-Z. Teng, Non-traditional fractionation of non-traditional isotopes: Evaporation, chemical diffusion and Soret diffusion. *Chem. Geol.* **258**, 92–103 (2009).

66. G. Lofgren, W. J. Russell, Dynamic crystallization of chondrule melts of porphyritic and radial pyroxene composition. *Geochim. Cosmochim. Acta* **50**, 1715–1726 (1986).

67. P. M. Radomsky, R. H. Hewins, Formation conditions of pyroxene-olivine and magnesian olivine chondrules. *Geochim. Cosmochim. Acta* **54**, 3475–3490 (1990).

68. S. J. Desch, M. A. Morris, H. C. Connolly, A. P. Boss, The importance of experiments: Constraints on chondrule formation models. *Meteorit. Planet. Sci*. **47**, 1139–1156 (2012).

69. L. L. Hood, Thermal processing of chondrule precursors in planetesimal bow shocks. *Meteorit. Planet Sci.* **33**, 97–107 (1998).

70. F. J. Ciesla, L. L. Hood, S. J. Weidenschilling, Evaluating planetesimal bow shocks as sites for chondrule formation. *Meteorit. Planet Sci.* **39**, 1809–1821 (2004).

71. J. A. Wood, Processing of chondritic and planetary material in spiral density waves in the nebula. *Meteorit. Planet Sci.* **31**, 641–645 (1996).

72. A. P. Boss, R. H. Durisen, Chondrule-forming shock fronts in the solar nebula: A possible unified scenario for planet and chondrite formation. *Astrophys. J.* **621**, L137–L140 (2005).

73. F. H. Shu, H. Shang, T. Lee, Toward an astrophysical theory of chondrites. *Science* **271**, 1545–1552 (1996).

74. W. Pilipp, T. W. Hartquist, G. E. Morfill, Eh. Levy, Chondrule formation by lightning in the Protosolar Nebula? *Astron. Astrophys*. **331**, 121–146 (1998).

75. S. J. Desch, J. N. Cuzzi, The generation of lightning in the solar nebula. *Icarus* **143**, 87–105 (2000).

76. J.-D. Bodénan, C. Surville, J. Szulágyi, L. Mayer, M. Schönbächler, Can chondrules be produced by the interaction of Jupiter with the protosolar disk? *Astrophys. J.* **901**, 60 (2020).

77. C. R. Mann, A. C. Boley, M. A. Morris, Planetary embryo bow shocks as a mechanism for chondrule formation. *Astrophys. J.* **818**, 103 (2016).

78. N. X. Nie, N. Dauphas, T. Hopp, J.-Y. Hu, Z. J. Zhang, R. Yokochi, T. Ireland, F. L. Tissot, Chromatography purification of Rb for accurate isotopic analysis by MC-ICPMS: a comparison between AMP-PAN, cation-exchange, and Sr resins. *J. Anal. At. Spectrom.* (2021).

79. T. J. Ireland, F. L. H. Tissot, R. Yokochi, N. Dauphas, Teflon-HPLC: A novel chromatographic system for application to isotope geochemistry and other industries. *Chem. Geol.* **357**, 203–214 (2013).

80. N. Dauphas, F. L. H. Tissot, R. Yokochi, T. J. Ireland, U.S. Patent US20150008171A1 (2015); https://patents.google.com/patent/US20150008171A1/en.

81. A. V. Fedkin, L. Grossman, F. J. Ciesla, S. B. Simon, Mineralogical and isotopic constraints on chondrule formation from shock wave thermal histories. *Geochim. Cosmochim. Acta* **87**, 81–116 (2012).

82. J. M. Friedrich, M. K. Weisberg, D. S. Ebel, A. E. Biltz, B. M. Corbett, I. V. Iotzov, W. S. Khan, M. D. Wolman, Chondrule size and related physical properties: A compilation and evaluation of current data across all meteorite groups. *Geochemistry* **75**, 419–443 (2015).

83. J. L. Gooding, K. Keil, Relative abundances of chondrule primary textural types in ordinary chondrites and their bearing on conditions of chondrule formation. *Meteoritics* **16**, 17–43 (1981).

84. C. M. O. Alexander, D. S. Ebel, Questions, questions: Can the contradictions between the petrologic, isotopic, thermodynamic, and astrophysical constraints on chondrule formation be resolved? *Meteorit. Planet Sci.* **47**, 1157–1175 (2012).

85. B. R. Frost, Introduction to oxygen fugacity and its petrologic importance, in *Oxide Minerals* (De Gruyter, 2018), pp. 1–10.

86. B. Bourdon, C. Fitoussi, Isotope fractionation during condensation and evaporation during planet formation processes. *ACS Earth Space Chem.* **4**, 1408–1423 (2020).

87. H. Y. McSween Jr., Chemical and petrographic constraints on the origin of chondrules and inclusions in carbonaceous chondrites. *Geochim. Cosmochim. Acta* **41**, 1843–1860 (1977).

88. J. T. Wasson, G. W. Kallemeyn, Compositions of chondrites. *Philos. Trans. R. Soc., A* **325**, 535–544 (1988).

89. R. H. Hewins, M. Bourot-Denise, B. Zanda, H. Leroux, J.-A. Barrat, M. Humayun, C. Göpel, R. C. Greenwood, I. A. Franchi, S. Pont, J.-P. Lorand, C. Cournède, J. Gattacceca, P. Rochette, M. Kuga, Y. Marrocchi, B. Marty, The Paris meteorite, the least altered CM chondrite so far. *Geochim. Cosmochim. Acta* **124**, 190–222 (2014).

90. H. Y. McSween, Alteration in CM carbonaceous chondrites inferred from modal and chemical variations in matrix. *Geochim. Cosmochim. Acta* **43**, 1761–1770 (1979).

91. H. Y. McSween Jr., Carbonaceous chondrites of the Ornans type: A metamorphic sequence. *Geochim. Cosmochim. Acta* **41**, 477–491 (1977).

92. H. Y. Mcsween Jr., Petrographic variations among carbonaceous chondrites of the Vigarano type. *Geochim. Cosmochim. Acta* **41**, 1777–1790 (1977).

93. J. Bayron, I. Erb, D. Ebel, S. Wallace, H. Connolly, Modal abundances and chemistry of clasts in the Renazzo (CR2) chondrite by x-ray map analysis, in *Proceedings of the 45th Annual Lunar and Planetary Science Conference*, Woodlands, TX, USA (17 to 21 March 2014), p. 1225.

4. D. L. Schrader, I. A. Franchi, H. C. Connolly Jr., R. C. Greenwood, D. S. Lauretta, J. M. Gibson, The formation and alteration of the Renazzo-like carbonaceous chondrites I: Implications of bulk-oxygen isotopic composition. *Geochim. Cosmochim. Acta* **75**, 308–325 (2011).

95. A. I. Blinova, T. J. Zega, C. D. K. Herd, R. M. Stroud, Testing variations within the Tagish Lake meteorite—I: Mineralogy and petrology of pristine samples. *Meteorit. Planet Sci.* **49**, 473–502 (2014).